

Lateral flow of thick continental lithospheric mantle during tectonic quiescence

Claudio Alejandro Salazar-Mora^{a,b,*}, Victor Sacek^b

^a Instituto de Geociências, Universidade de São Paulo, Rua do Lago, 562, 05508-080, São Paulo, Brazil

^b Instituto de Astronomia, Geofísica e Ciências Atmosféricas, Universidade de São Paulo, Rua do Matão, 1226, 05508-090, São Paulo, Brazil

ARTICLE INFO

Keywords:

Numerical modelling
Density contrasts
Cratonic lithosphere
Orogenic lithosphere
Tectonic quiescence

ABSTRACT

The amalgamation of continental blocks naturally results in a lithosphere with lateral variations in thickness due to the juxtaposition of thicker cratonic and thinner orogenic lithospheres, which in turn evolve together through time. After the amalgamation, this mosaic of continental blocks can experience longstanding periods of relative tectonic quiescence until the next tectonic event, for instance continental rifting. Using geodynamic numerical models, we explored the internal deformation of the continental lithosphere during periods of tectonic quiescence taking into account lateral variations of lithospheric thickness. We observed that the orientation of lateral flow of the thick cratonic lithosphere depends primarily on the compositional density contrasts ($\Delta\rho$) between the asthenosphere and continental lithospheric mantle and on the width of the juxtaposed mobile belt lithosphere. In the case of mobile belts wider than 300 km, the margin of the thick craton flows towards (or underplates) the base of the thin lithosphere when $\Delta\rho \geq 32\text{--}48\text{ kg/m}^3$, whereas for smaller $\Delta\rho$ values, the thick cratonic margin flows away from mobile belt, preserving a sharp thickness variation. For mobile belts narrower than 300 km, the $\Delta\rho$ threshold between underplate or outward behavior decreases with the mobile belt width. Underplating of cratonic lithosphere beneath the thin lithosphere is efficient in mobile belts narrower than 300 km and for higher $\Delta\rho$, which allows them to cool, thicken and stiffen. Lateral flow of cratonic lithosphere is not efficient to underplate wide mobile belts thoroughly, so the latter are influenced by asthenospheric heat for prolonged periods and thus remain less rigid. Therefore, we propose that protracted tectonic quiescence of supercontinents can develop lithospheric rheological inheritances that may or may not facilitate post-quiescence continental lithospheric rifting.

1. Introduction

During tectonic quiescence, the effects of tectonic forces that cause contraction or extension within the continental lithosphere are limited or even imperceptible in the geological record. At the same time, the base of the continental lithosphere is constantly interacting with the underlying asthenospheric mantle. Due to the irregular shape of the base of the continental lithosphere, small-scale convection in the asthenosphere can be driven by the lateral variation in lithospheric thickness (King and Anderson, 1998). Conversely, the vigor of the asthenospheric flow can reshape the base of the continental lithosphere, depending on the rheological structure and density distribution in the upper mantle. Besides temperature, compositional heterogeneity in the lithospheric mantle is a key factor controlling density variations (Doin et al., 1997; Foley, 2008; King, 2005), which is attested by extensive petrological and

geochemical analyses of worldwide mantle xenoliths (Pearson and Wittig, 2014). Water content in olivine crystals brought from the lithospheric mantle also confirms compositional heterogeneity between the lithospheric mantle beneath thick and thin continental lithosphere (Peslier and Luhr, 2006).

Compositional density diversity is thought to be the result of secular variations in the composition and mineralogy of the lithospheric mantle through Earth's history (Griffin et al., 1998). Chemical, petrological and experimental constraints from mantle-derived peridotites permitted the determination of mean densities (STP conditions) for the lithospheric mantle (LM) as a function of age (Fig. 1). Griffin et al. (1998) obtained 3310 kg/m^3 for Archean LM, 3330 kg/m^3 for Proterozoic LM and 3354 kg/m^3 for Phanerozoic LM. Similarly, Poudjom Djomani et al. (2001) obtained 3310 kg/m^3 for Archean LM, 3350 kg/m^3 for Proterozoic LM and 3360 kg/m^3 for Phanerozoic LM. Considering the relationship of

* Corresponding author at: Instituto de Geociências, Universidade de São Paulo, Rua do Lago, 562, 05508-080, São Paulo, Brazil.

E-mail address: claudio.mora@usp.br (C.A. Salazar-Mora).

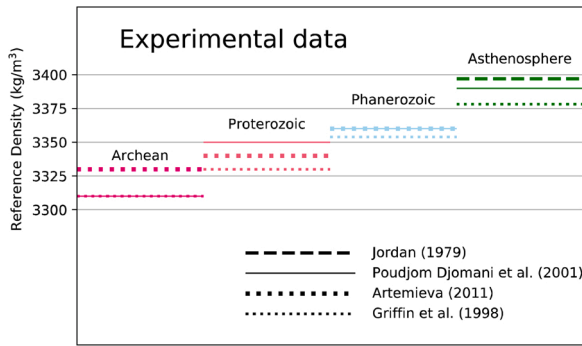


Fig. 1. Range of reference densities for the continental lithospheric mantle (for Archean, Proterozoic and Phanerozoic) and for the asthenosphere (green).

lithospheric density and Mg#, Artemieva (2011) obtained 3330 kg/m^3 for Archean LM, 3340 kg/m^3 for Proterozoic LM and 3360 kg/m^3 for Phanerozoic LM. In the case of the asthenosphere, density values are calculated considering the *pyrolite* model (Ringwood, 1975). Distinctive *pyrolite* compositions can be assumed depending on the comparison of natural rocks from diverse natural situations (see Green and Falloon, 1998 for a review). Widely mentioned calculated values are 3397 kg/m^3 (Jordan, 1979), 3390 kg/m^3 (Poudjom Djomani et al., 2001) and 3378 kg/m^3 (Griffin et al., 1998).

Better constraints on density contrasts ($\Delta\rho$) between asthenospheric and lithospheric mantle are essential in geodynamic models since it is already known that this kind of contrast influences continental lithosphere stability (e.g. Lee et al., 2011; Currie and van Wijk, 2016). Considering the density values obtained by Griffin et al. (1998), the mean density contrast for the Archean is $\Delta\rho_{\text{arc}} = 68 \text{ kg/m}^3$, for the Proterozoic is $\Delta\rho_{\text{prt}} = 48 \text{ kg/m}^3$, and for the Phanerozoic is $\Delta\rho_{\text{pha}} = 24 \text{ kg/m}^3$.

Lateral variations in continental lithosphere thickness have long been recognized particularly due to deep cratonic roots (e.g. Jordan, 1978). Estimates of the thermal thickness show that Archean cratonic lithosphere varies from 200–220 km to > 300 km, while Precambrian lithosphere can vary from 200 km to ~140 km (Artemieva and Mooney, 2002). Surface-wave tomography studies (e.g. Priestley et al., 2018) show that thick lithosphere (~200–220 km) is present under cratonic regions and that thin lithosphere (<140 km) under tectonically active regions. Lithospheric thickness compilations by Artemieva (2011) show that Proterozoic orogens from south and central Africa and Paleozoic orogens like the Caledonides and the Appalachians show lithospheric thicknesses between 100–150 km, while Cenozoic active mobile belts vary from 80–150 km in lithospheric thickness, when the downgoing slabs are excluded. The seismically observed lateral lithospheric thickness variation between mobile belt and adjacent craton is up to 200 km in the Meso-Cenozoic Canadian Cordillera (Chen et al., 2019) and 150 km in the European Sorgenfrei-Tornquist Zone (Hieronymus et al., 2007).

In this paper we present geodynamic numerical models that aimed to test the sensitivity of density contrasts between the lithospheric mantle and the asthenosphere over long-lived periods of tectonic quiescence, evaluating how compositional density differences affected the evolution of the base of the continental lithosphere that comprises neighboring thick and thin lithospheric domains. Previous research has shown that the longevity and stability of thicker lithospheric domains can be disturbed by edge-driven convection provided that lithospheric lateral variations in thickness trigger small-scale convection (King and Anderson, 1998). If not disturbed by its edges, deep roots can be influenced by upward asthenospheric flux or undergo delamination, the latter case being mainly caused by permanent compositional change (Foley, 2008). However, it is still unclear how thicker domains of continental lithosphere behave alongside thinner domains during prolonged periods of

quiescence. As it is depicted by Western Gondwana Supercontinent, for example, where at least 300 Myr have passed since its amalgamation (Schmitt et al., 2018) until its onset of rifting (Cainelli and Mohriak, 1999), quiescence may last hundreds of millions of years, a period over which thick and old cratonic keels and younger thin lithospheric domains remain juxtaposed.

2. Numerical modelling and setup

The numerical simulation of the mantle convection to reproduce the evolution of cratonic and orogenic lithosphere interacting with the sublithospheric mantle involves the solution of the following differential equations related to the conservation laws of mass, energy and momentum, respectively (Zhong et al., 2007):

$$u_{i,i} = 0$$

$$\partial T / \partial t + u_i T_{,i} = \kappa T_{,ii} + H/c_p + u_i g_i \alpha T/c_p$$

$$\sigma_{ij,j} + g_i \rho = 0$$

where

$$\sigma_{ij} = -P \delta_{ij} + \eta(u_{i,j} + u_{j,i})$$

$$\rho = \rho_0 (1 - \alpha(T - T_0))$$

u_i is the component i of the velocity field, T is temperature, t is time, κ is the thermal diffusivity, H is heat production per unit mass, c_p is the specific heat capacity, g is gravity, ρ is the effective rock density dependent on temperature and composition, ρ_0 is the reference rock density at temperature T_0 , α is the coefficient of thermal expansion, P is the dynamic pressure, η is the effective viscosity, and δ_{ij} is the Kronecker delta (see Table 1). Repeated indexes mean summation and index after comma represent partial derivative to the respective spatial coordinate. The last term in the energy equation represents the temperature correction due to adiabatic heating.

In the present paper, we used a modified version of the software presented in Sacek (2017), incorporating internal heat production due to radiogenic decay and adiabatic heating. Additionally, Lagrangian markers are used to track compositional differences in the model. To construct and solve the linear system associated with the finite element approach, we make use of PETSc (the Portable, Extensible Toolkit for Scientific Computation) (Balay et al., 2018) and to validate the present numerical model, the code was benchmarked against models presented by van Keken et al. (1997).

The effective viscosity η is given by the Frank-Kamenetskii approximation (Solomatov and Moresi, 2000):

$$\eta = f \eta_r b \exp[-\gamma T],$$

where η_r is a reference viscosity, f is a compositional scale factor for viscosity, and b and $\gamma = E_a/RT_b^2$ are constants. E_a is the activation energy, R is the gas constant, and T_b is the basal temperature. Both T and T_b are

Table 1
Input parameters for the numerical simulations.

Parameter	Description	Value
α	Thermal expansion coefficient	$3.28 \times 10^{-5} \text{ } ^\circ\text{C}^{-1}$
κ	Thermal diffusivity	$1.0 \times 10^{-6} \text{ m}^2/\text{s}$
c_p	Specific heat capacity	$1250 \text{ J kg}^{-1} \text{ K}^{-1}$
g	Acceleration of gravity	10 m/s^2
E_a	Activation energy	240 kJ/mol
R	Gas constant	8.31 J/mol K
T_b	Basal temperature	$1500 \text{ } ^\circ\text{C}$
T_0	Top temperature and reference temperature	$0 \text{ } ^\circ\text{C}$
η_r	Reference viscosity	10^{19} Pa.s
b	Nondimensional pre-exponent	10^7
L_x	Model domain x-direction	1600 km
L_z	Model domain z-direction	660 km

in Kelvin in the expression for the effective viscosity.

We assumed a two-dimensional domain (Fig. 2a) with 1600 km in the horizontal direction and 660 km in depth, subdivided into $200 \times 80 = 16,000$ elements. The initial thermal structure (Fig. 2) in the lithosphere is close to a steady state condition for thermal conduction taking into account the variable heat production in the crust and lithospheric mantle (see Table 1). For this initial temperature condition, we simulated a simple 2D thermal conduction model using a finite difference code in Python (see supplementary material), assuming that the temperature at the top is fixed at T_0 and the irregular bottom of the lithosphere was maintained at 1300°C , with the initial temperature decreasing linearly with depth. This 2D model takes into account vertical and lateral heat conduction along with radiogenic heat production. This conductive model is performed for 100 Myr and the final thermal structure assumed as the initial condition for the thermomechanical model. With this procedure, we avoid sharp lateral variations of temperature at the walls of the cratonic margins with the adjacent asthenosphere at the onset of the thermomechanical simulation (see Fig. 2a). In the asthenosphere, we adopted an adiabatic increase in temperature as in the following expression:

$$T_{\text{initial}}(z) = T_p \exp(g \alpha z/c_p),$$

where z is the vertical spatial coordinate and $T_p = 1262^\circ\text{C}$ is the mantle potential temperature.

In the onset of the numerical simulation (Fig. 2a), we assumed that the lithospheric thickness L of 250 km represents the cratonic lithosphere (e.g. Artemieva and Mooney, 2002), while in the central portion of the model a thin lithospheric domain (TL) is 100 km thick with a width W_{TL} . The thin lithosphere represents the mean thermal lithospheric thickness of Neoproterozoic, Paleozoic and Cenozoic orogenic belts, excluding the downgoing slabs (Artemieva, 2011). Free slip was assumed in all boundaries of the model and the temperature at the top and at the bottom of the model were maintained constant.

The lithospheric mantle is assumed compositionally distinct from the sublithospheric one, with a different reference density and viscosity scale factor f , where we assumed a higher viscosity factor for the lithospheric mantle in comparison to the asthenospheric one (e.g. Peslier et al., 2010). We tested different widths W_{TL} , density contrasts between sublithospheric and lithospheric mantle, and viscosity scale factor, to evaluate how these parameters affect the geometry of the base of the lithosphere at the cratonic edge, close to the thin lithosphere domain (see Table 2). The numerical simulation is performed for a period of 300 Myr and the geometric pattern of the base of the lithospheric mantle at the transition between the cratonic and thin lithosphere is observed through time.

3. The effects of density contrasts on cratonic lithospheric mantle flow

Our models show that not only the thermal gradients between the

lithosphere and the sublithospheric mantle can shape the cratonic borders. Instead, the density contrasts between lithospheric and sublithospheric mantle due to secular compositional differences causes the cratonic margin to laterally flow in respect to the neighboring sublithospheric mantle beneath the thin lithosphere (Figs. 3 and 4). The inward and outward flow are defined as the cumulative displacement of the cratonic particles at the end of the numerical simulation, i.e. 300 Myr after the onset of the experiment.

Fig. 3 shows the accumulated behavior of the cratonic margins after 300 Myr of quiescence in respect to a confined 200 km wide thin lithospheric domain. In these numerical experiments we assumed that the compositional factor f is 100 for the lithospheric mantle while for the asthenosphere is 1, making the lithospheric mantle 100 times more viscous than the asthenosphere at the same temperature. The typical density contrasts adopted hereafter for the Archean is $\Delta\rho_{\text{arc}} = 68 \text{ kg/m}^3$, for the Proterozoic $\Delta\rho_{\text{prt}} = 48 \text{ kg/m}^3$ and for the Phanerozoic $\Delta\rho_{\text{pha}} = 24 \text{ kg/m}^3$.

In the case of $\Delta\rho_{\text{arc}} = 68 \text{ kg/m}^3$ (Fig. 3a), the density contrast causes the cratonic margins to flow inwards to the thinner domain, developing cratonic lithosphere bulges towards the center of the thinner domain, which in turn reduces the sharp lateral variation of lithospheric thickness. As a consequence, under this area, small-scale convections from the sublithospheric mantle are precluded and conductive cooling of the lithosphere is favored. The right column in Figs. 3 and 4 show plots of the depth of the lithospheric thermal base as a function of time, which were computed over a width of 80 km centered in the middle of the model domain. The depth of this thermal boundary layer is determined by the intersection of the linear adjustment of the temperature profile in the sublithospheric mantle with the same adjustment in the lithospheric mantle. The plots in Fig. 3a and b show that in the center of the model the thermal thickness is doubled (from ~ 110 km to ~ 220 km) after > 220 Myr of tectonic quiescence.

For density contrasts of 48 kg/m^3 , which is the Proterozoic average, the cratonic margin still flows inwards, but the flow is less pronounced than models with Archean density contrasts (Fig. 3b). The change of the cratonic lithospheric mantle flow begins around density contrasts $\leq 30 \text{ kg/m}^3$, when the main behavior shifts to *outward flow*. For a typical Phanerozoic density contrast of 24 kg/m^3 (Fig. 3c), it is observed that the cratonic margins tend to flow outwards, that is, away from the orogenic domain, causing it to thicken in the vicinities of the thinner domain and preserving the lateral variation in thickness. A small-scale convective pattern is established below the thin lithosphere domain after 125 Myr (see Animation 1 in the supplementary material), when advective heating prevails and precludes the orogenic lithosphere to thermally thicken by conductive cooling (Fig. 3c).

4. The effects of the thin lithospheric domain width

In order to explore the flow of the cratonic lithosphere during a period of quiescence for different widths of the thin lithospheric domain, over 200 simulations were carried out for narrow (< 300 km) and wide

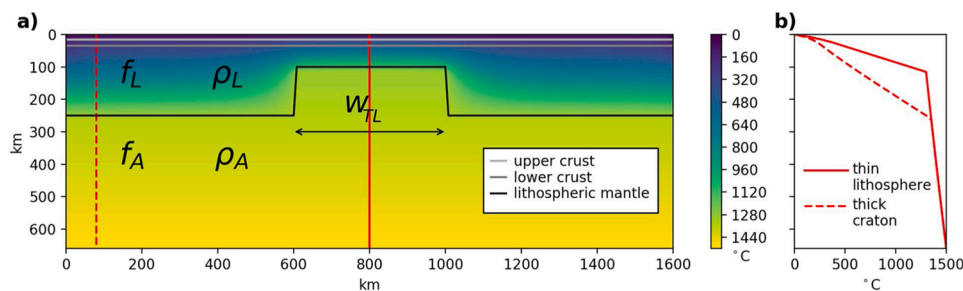


Fig. 2. a) Initial thermal and compositional structure for the numerical scenarios, where f_L and ρ_L are viscosity scaling factor and density of the lithosphere, respectively. Similarly, f_A and ρ_A refer to the asthenosphere. W_{TL} is the width of the thin lithosphere domain, which in this example is 400 km. Both upper and lower crust are 15 km thick. b) Initial thermal profile for the thin and thick lithospheres. The positions of these thermal profiles are indicated in Fig. 2a.

Table 2
Specific parameters for the different layers in the models.

Description	Parameter	Upper crust	Lower crust	Lithospheric mantle	Asthenospheric mantle
Density	ρ	2700 kg/m ³	2800 kg/m ³	3310–3354 kg/m ³	3378 kg/m ³
Heat production	H	9.2×10^{-10} W/kg	2.9×10^{-10} W/kg	1.0×10^{-12} W/kg	0.0 W/kg
Viscosity scaling factor	f	1	1	100–500	1
Width of the thin lithosphere	W_{TL}	100–800 km	100–800 km	100–800 km	100–800 km

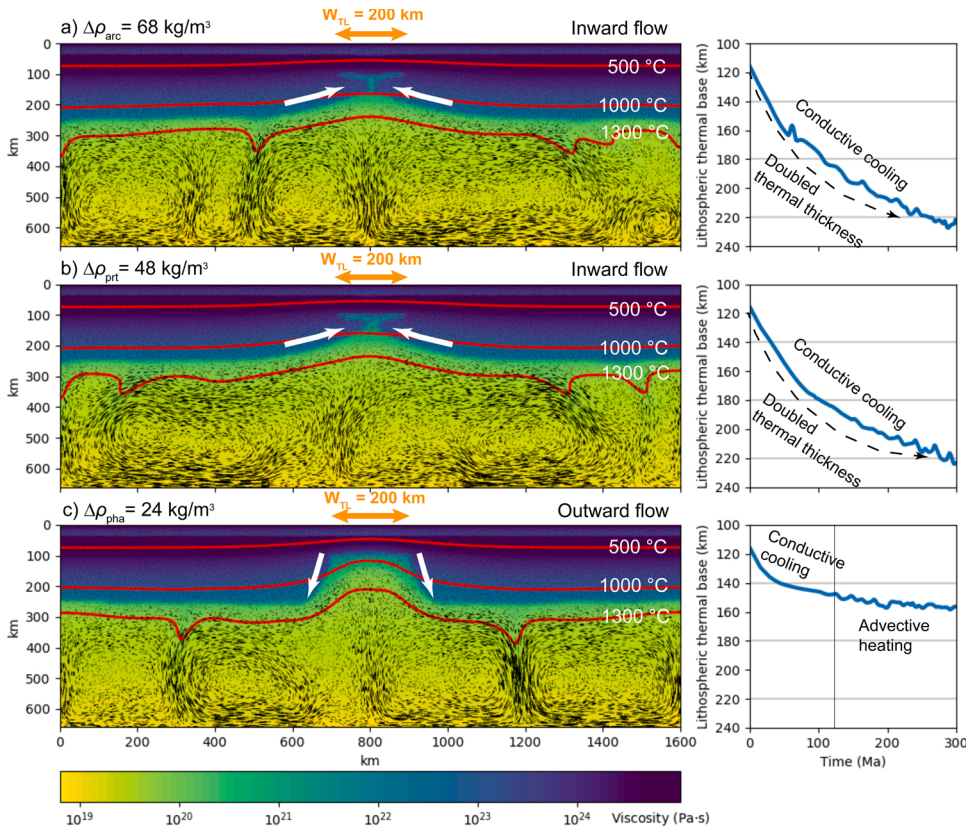


Fig. 3. Behavior of the thick cratonic lithosphere margin in respect to the thin lithosphere domain with $W_{TL} = 200$ km after 300 Myr of tectonic quiescence (left) and plots of the depth to the base of the thermal boundary layer under the thin lithosphere domain as a function of time (right). The sharp transition in viscosity represents the boundary between lithosphere (blue) and asthenosphere (greenish-yellow). In the three scenarios, the compositional factor f in these models is 100 for the lithospheric mantle and 1 for the asthenosphere. The numerous thin black curves represent the movement of mantle particles during a time interval of 500 kyr. a) lithospheric mantle flows inward the thinner lithosphere (white arrows), with $\Delta\rho_{arc}$ representing Archean lithosphere; b) inward flow (white arrows) of the lithospheric mantle with smaller density contrasts ($\Delta\rho_{prt}$), typical of Proterozoic times, showing a less pronounced inward cratonic migration; and c) lithospheric mantle flows outward (white arrows) due to smaller density contrast for the Phanerozoic ($\Delta\rho_{pha}$), allowing for sub-lithospheric mantle convecting cells beneath the orogenic lithosphere and advective heating from 125 to 300 Myr. See animations in the supplementary material.

thin regions (>300 km).

The behavior of the cratonic margins for wide thin lithospheric domains (600 km wide) is shown in Fig. 4. The main difference in respect to narrower areas is that advective heating from the mantle dominates in the center of the model, regardless of the inward or outward flow.

In this matter, the inward flow of typically Archean cratonic margin does not preclude the action of mantle convective cells beneath the mobile belt, which in turn, prevents the thinner lithosphere from conductively thickening to more than 160 km (Fig. 4a).

Comparing the six scenarios in Figs. 3 and 4, it is worth noting that the density contrast is effective in controlling lithospheric flow. The difference in respect to narrow thin domains (Fig. 3), is that in wider ones (Fig. 4) the advective heating is responsible for keeping the thinner lithosphere hotter and softer for a longer period of time during tectonic quiescence. In the case of $\Delta\rho_{pha}$, the outward cratonic margin flow causes the migrated cratonic margin to be partially eroded to the mantle by edge-driven convection (Fig. 4c; see Animation 3 in the supplementary material), which is observed to be more vigorous in wider thin lithospheric domains than in narrower ones (e.g. Fig. 3c).

The style of flow of the lithospheric mantle accumulated after 300 Myr of tectonic quiescence was tested for varying $\Delta\rho$ and thin regions widths and the results were classified as *inward* or *outward* flow. Another parameter varied was the scaling factor for viscosity (f) of the lithosphere. Fig. 5a presents all the simulated models considering a lithospheric mantle scaling factor of $f_L = 100$ and a sublithospheric one of f_A

$= 1$. In the case of wide thin regions (≥ 300 km), the shift from purely *outwards* to *inward* field is constant around ~ 32 kg/m³. In Fig. 5b and c the models are plotted with $f_L = 250$ and $f_L = 500$, respectively. The increase in lithospheric viscosity caused the increase of the inward/outward $\Delta\rho$ limit, where $f_L = 250$ is associated to $\Delta\rho = \sim 36$ kg/m³ and $f_L = 500$ to $\Delta\rho = \sim 48$ kg/m³. For the narrow thin regions (≤ 300 km), the shift is shown to be dependent on width, where the $\Delta\rho$ threshold between fields increases for wider regions. Another interesting observation is that the lithospheric viscosity controls the extent to which the inward flow can reach. Less viscous cratonic lithosphere (e.g. $f_L = 100$) can flow inwards for more than 100 km in the scenarios with $\Delta\rho > 50$ kg/m³, whereas the lateral flow for high viscous cratonic lithosphere (e.g. $f_L = 500$) is limited to a few tens of kilometers in a time interval of 300 Myr.

5. Discussion

The lateral variation in thickness of the continental lithosphere is an important feature of large continental masses and how this thickness evolves during periods of tectonic quiescence is still rather unexplored. The erosion of cratonic lithospheric keels due to mantle dynamics has been shown to depend on the thermal gradient between continental lithospheric mantle and asthenosphere (Artemieva, 2011) as well as on the cratonic lithosphere thickness. If the cratonic roots are too deep (~ 350 km), marginal erosion occurs from the sides, whereas thinner roots (~ 220 km) tend to be eroded from below (Doin et al., 1997; Lee

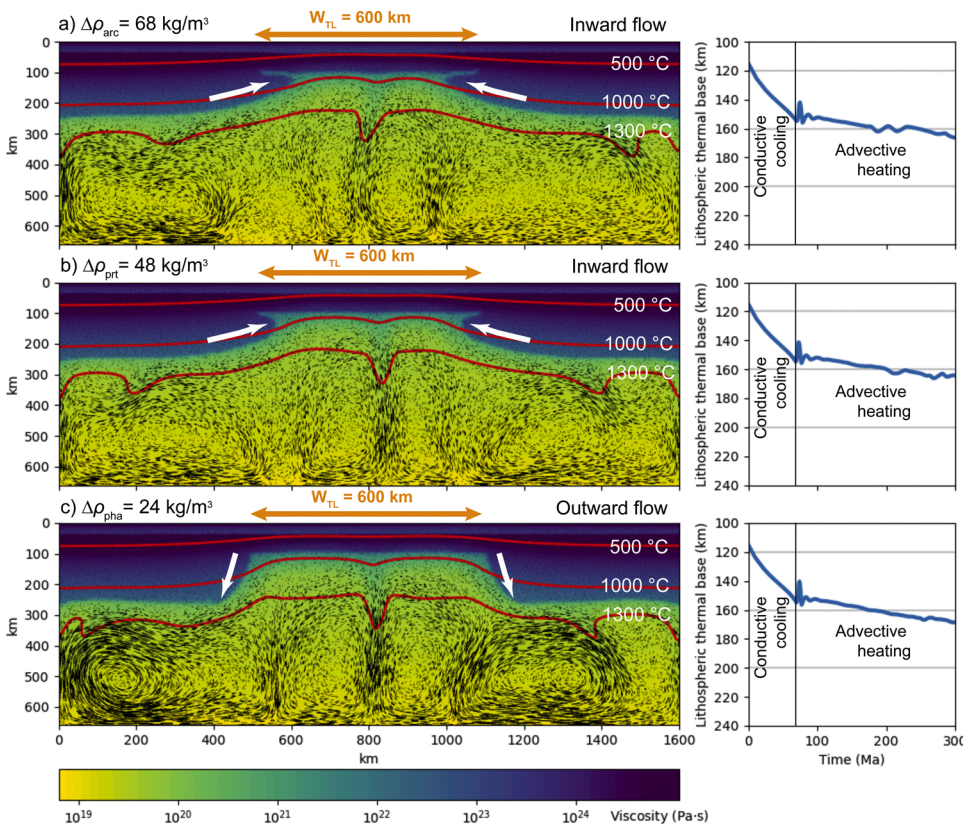


Fig. 4. For $W_{TL} = 600$ km and 300 Myr of quiescence, models show that advective heating takes place regardless of the cratonic margin flow (see right-side plots). The numerous thin black curves represent the movement of mantle particles during a time interval of 500 kyr. In the three scenarios, the compositional factor f in these models is 100 for the lithospheric mantle and 1 for asthenosphere. a) Inward flow (white arrows) of the cratonic lithosphere, for Archean density contrasts. b) Less pronounced cratonic margin bulge due to inward flow for Proterozoic density contrasts. c) Outward flow of the margins with Phanerozoic density contrasts. Note that for all models, conductive cooling thickened the thin lithosphere domain until < 160 km, after which advective heating keeps it with nearly constant thickness.

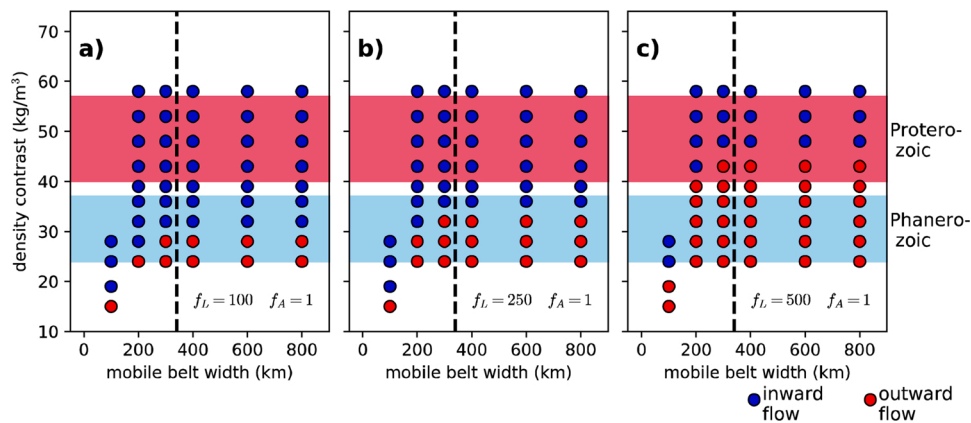


Fig. 5. Plots of $\Delta\rho$ versus W_{TL} showing the type of flow (inward or outward) of the cratonic lithosphere in respect to the thin lithosphere domain. f_L and f_A are the viscosity scaling factor for the lithosphere and the asthenosphere, respectively. Narrow mobile belts are plotted to the left of the vertical dashed lines, where $\Delta\rho$ threshold between inward and outward flow decreases with mobile belt width.

et al., 2011). Previous studies (e.g. Currie and van Wijk, 2016; King and Anderson, 1998) underline the importance of a steep gradient in lithospheric thickness between craton and adjacent continent and how its relationship with density contrasts influence cratonic margin erosion. Our numerical models went further in showing that both density contrasts between asthenospheric and lithospheric mantle as well as the width of the mobile belt lithosphere control cratonic margin lateral flow.

5.1. Physical explanation for the sense of lateral flow at cratonic margins

The inward or outward flow of the cratonic mantle depends on the effective density difference between the asthenosphere and the lithospheric mantle. The effective density difference depends not only on the compositional density difference $\Delta\rho$ but also on the temperature

contrast. As the lithospheric mantle is colder than the asthenosphere, the transition between inward and outward flow occurs when the compositional density contrast is positive ($\Delta\rho > 0$) i.e., the lithospheric mantle is compositionally less dense than the asthenosphere, therefore compensating the density change due to temperature difference.

Qualitatively, when the effective density of the cratonic lithosphere is smaller than the asthenospheric one, the cratonic lithosphere tends to move upward, flowing inward to the base of the mobile belt lithosphere. Conversely, the outward (and downward) flow occurs when the effective density of the lithospheric mantle is larger than the asthenospheric one.

The transition between inward and outward flow is also dependent on mobile belt width for $W_{TL} < 400$ km because, in these scenarios, the asthenospheric mantle under the narrow mobile belt is not effectively

recycled by convection, turning this portion of the asthenosphere slightly colder, diminishing the temperature contrast between asthenosphere and cratonic mantle. In these cases, the transition between inward and outward flow can occur when the compositional density contrast $\Delta\rho$ is smaller.

Finally, the effective viscosity of the lithosphere also affects the position of the inward/outward flow transition. This occurs due to an indirect effect of the effective viscosity on the thermal structure of the lithosphere, where in the models with higher effective viscosity ($f_L = 500$, Fig. 4c) and consequently more rigid lithosphere, the conductive cooling predominates, resulting in thicker and colder lithosphere. With a higher temperature difference between the cratonic lithosphere and the adjacent asthenosphere, the inward/outward transition occurs at a larger compositional density contrast $\Delta\rho$.

The use of other rheological laws, including non-linear flow like dislocation creep rheology, can also modify the effective viscosity of the mantle, and consequently affecting the position of the inward/outward flow transition. However, we expect that if different rheological laws result in similar effective viscosity structure for the mantle, the inward/outward flow pattern will be compatible.

5.2. Density contrasts ($\Delta\rho$), lithospheric viscosity and mobile belt width (W_{TL})

Mobile belts with typical Proterozoic $\Delta\rho$ ($\sim 48 \text{ kg/m}^3$) tend to have its marginal cratonic lithosphere flowing *inwards* (Fig. 5). On the other hand, when wide belts (i.e. $> 300 \text{ km}$ wide) are simulated with typical Phanerozoic $\Delta\rho$ ($\sim 28 \text{ kg/m}^3$), those models show an increasing tendency to *outward* flow of the marginal cratonic lithosphere. The density contrasts are thus a primary controlling factor of the cratonic lateral flow during tectonic quiescence, once they affect both narrow and wide mobile belts. The decrease in density contrasts is a result of the secular increase of the lithospheric mantle density, which has important implications for testing geodynamic scenarios during different periods of Earth's evolution. For instance, assuming typical Proterozoic $\Delta\rho$ (i.e. $\sim 48 \text{ kg/m}^3$) to model present-day wide orogens and their neighboring cratons would not be reasonable.

The viscosity of the lithospheric mantle is also important, where the higher the viscosity, the higher the inward/outward threshold in wide mobile belts. The content of water is one of the main factors controlling cratonic keels resistance to asthenospheric erosion, where dehydrated cratonic lithospheric mantle can be thousands of times more viscous than hydrated lithospheric mantle at the same temperature and pressure conditions (e.g. Peslier et al., 2010). Cratonic domains that have been influenced by Phanerozoic subductions tend to be more hydrated (e.g.

Lee et al., 2011) than old stable cratonic regions that were long dehydrated by melting and crustal recycling (e.g. Pollack, 1986). The density contrasts of the Proterozoic lithospheric mantle range between $40\text{--}58 \text{ kg/m}^3$ and our models show that for $f_L = 500$ the inward/outward threshold is $\Delta\rho = 48 \text{ kg/m}^3$ (see Fig. 5). With even higher viscous lithosphere (e.g. $f_L = 1000$), all cratonic margins would flow outwards, which would preserve a sharp lateral thickness variation in the lithosphere. Phanerozoic lithospheric mantle $\Delta\rho$ ranges from 24 to 38 kg/m^3 , and our models with less viscous Phanerozoic lithosphere ($f_L = 100$) show the inward/outward threshold to be 32 kg/m^3 , which means that most of this less viscous lithosphere would flow outward, also preserving the sharp lithospheric thickness variation.

5.3. Rheological implications

As an implication to the overall structure of the continental lithosphere (i.e. adjacent cratonic and orogenic lithospheres), the inward flow of cratonic lithosphere in narrow mobile belts favors the conductive cooling of the lithosphere and hence its increase in thickness. Fig. 6 presents yield strength envelopes (YSE's) for the six scenarios shown in Figs. 3 and 4, after 300 Myr of quiescence at the center of the model. For narrow belts ($W_{TL} = 200 \text{ km}$), the *inward* flow of the cratonic lithospheric mantle results in lithospheric stiffening (blue YSE's). This behavior is valid for $W_{TL} \leq 300 \text{ km}$ and for $\Delta\rho_{\text{arc}}$ and $\Delta\rho_{\text{prt}}$. On the other hand, *outward* flow enables advective heating at the base of the mobile belts, which hampers its conductive cooling, preserving its low rigidity. This is the case for $W_{TL} \geq 300 \text{ km}$, regardless of the lateral flow type and $\Delta\rho$ value (red YSEs).

In our numerical experiments, the flexural rigidity of the lithosphere is sensitive to density contrast only for models with relatively narrow mobile belts widths ($200\text{--}400 \text{ km}$, see Fig. 7). For example, for scenarios with mobile belt width of 200 km and $f_L = 100$, the increase of the density contrast from $\Delta\rho = 24 \text{ kg/m}^3$ to 53 kg/m^3 induced the increase in the effective elastic thickness from 51 to 64 km (Fig. 7). On the other hand, for models with wider mobile belts ($>400 \text{ km}$) the mean T_e is not sensitive to the density contrast between the lithospheric mantle and asthenosphere (Fig. 7). For the scenarios with narrow mobile belt width of 100 km , the thermal structure tends to become similar to the adjacent cratonic mantle, resulting in T_e values around 70 km and is less sensitive to density contrast.

Conductive cooling of the mobile belt lithosphere and its thermal thickening, along with volatile depletion that increases the stiffness of the deep keel, are effective factors controlling cratonization (Pollack, 1986), that is, turning the thinner lithosphere into a stable hard-to-deform (and melt) lithospheric domain. As a consequence, the

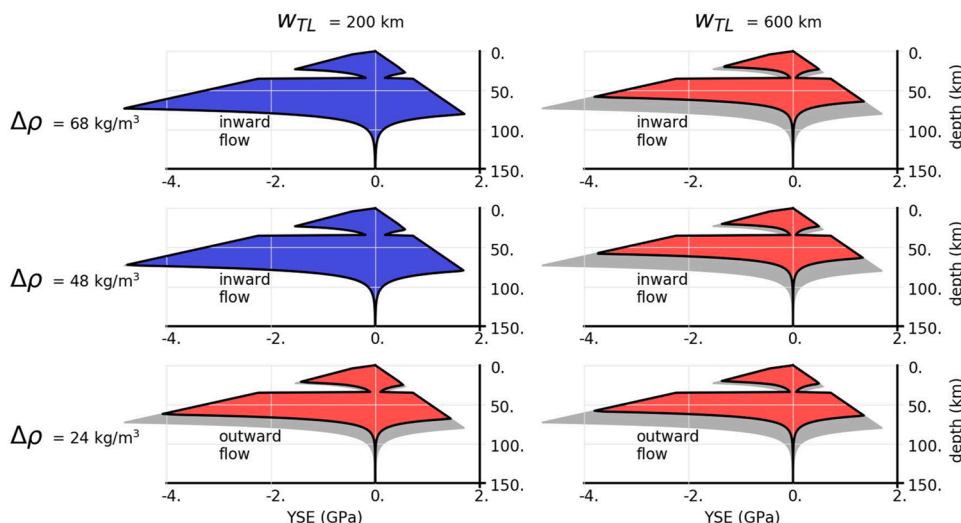


Fig. 6. Yield stress envelopes (YSE's) for the six scenarios shown in Figs. 3 and 4 after 300 Myr of quiescence. Negative yield stress represents compression. The blue YSE represent the models with significant lithospheric cooling and red YSE are the scenarios that preserved relatively thin lithosphere and consequently less rigid domains. The envelopes were constructed based on the thermal structure at the center of each model after 300 Myr of simulation. We assumed the creep flow law of the diabase for the crust and dry olivine for the mantle (Burov and Diament, 1995), with a strain rate of 10^{-17} s^{-1} . Additionally, the brittle limit is based on Byerlee's law, following the expressions presented by Burov and Diament (1995). To facilitate the comparison of the YSEs, we added the YSE for the scenario with $\Delta\rho = 68 \text{ kg/m}^3$ and mobile belt width of 200 km as a gray area in all the plots.

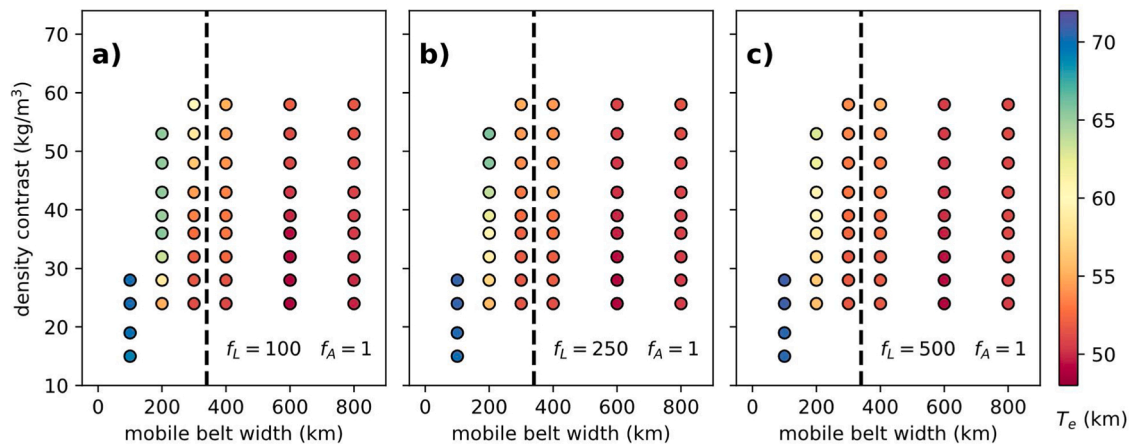


Fig. 7. The effective elastic thickness T_e of the mobile belt for numerical scenarios with different mobile belt widths and density contrasts. The mean thermal structure along the entire mobile belt was used to calculate the T_e . We assumed the creep flow law of the diabase for the crust and dry olivine for the mantle (Burov and Diament, 1995), with a strain rate of 10^{-17} s^{-1} . Additionally, the brittle limit is based on Byerlee's law, following the expressions presented by Burov and Diament (1995). For all the scenarios, we adopted the lithospheric curvature of $2 \times 10^{-7} \text{ m}$, with upward concavity. With this curvature, the crust is decoupled from the lithospheric mantle for all the scenarios presented in the three graphics and T_e was calculated as a two-layer lithosphere (Burov and Diament, 1995). Narrow mobile belts are plotted to the left of the vertical dashed lines, where the $\Delta\rho$ threshold between inward and outward flow decreases with mobile belt width.

overall structure of the continental lithosphere during a period of tectonic quiescence is heterogeneous in terms of thickness and rheology. A stronger and thermally thickened mobile belt domain is expected to hinder accumulation of strain (Audet and Bürgmann, 2011), while thinner lithosphere influenced by advective heating is maintained softened during tectonic quiescence, which would reasonably favor accumulation of strain (Gueydan et al., 2014). Strain localization is a key factor for the reactivation of inherited structures within the continental lithosphere during the onset of rifting, which could ultimately lead to continental breakup. Therefore, either strong or soft mobile belt lithosphere between cratonic blocks can develop a rheological inheritance during tectonic quiescence, which would be of great importance to the strength of large masses of continental lithosphere (e.g. supercontinents) upon subsequent rifting.

In practice, narrow mobile belts can strengthen the overall lithospheric structure of supercontinents for Proterozoic density contrasts after ~ 300 Myr of tectonic quiescence, whereas, for Phanerozoic density contrasts, narrow belts wider than 200 km produced thermally softened orogenic lithosphere within supercontinents (see Fig. 5a). As aforementioned, strong orogenic lithosphere delays or hinders strain accumulation, so their reactivation during supercontinent rifting must be aided by other types of tectonic inheritance (e.g. Salazar-Mora et al., 2018; Şengör et al., 2018) or mantle plume dynamics (Heron, 2018). In the case of wide mobile belts, the numerical results indicate that the behavior of the cratonic margin is independent of the width of the orogen and is essentially a function of the density contrast. Wide belts will always be thermally softened because the lateral flow extent of the surrounding cratonic keels is not sufficient to thermally separate the base of the orogenic lithosphere from the heat of the asthenosphere. Hence, very wide mobile belts (e.g. orogenic plateaus) contribute to the development of a continental lithosphere with marked rheologically different domains after tectonic quiescence.

5.4. Comparison to natural systems

The evolution of supercontinent Gondwana from its final assembly (Schmitt et al., 2018) in the transition between Ediacaran and Cambrian to its breakup (Cainelli and Mohriak, 1999) in the Mesozoic (a time span of ~ 300 Myr) can be envisaged in the context of Proterozoic $\Delta\rho$. One of the main orogens that was reactivated to permit continental breakup in Western Gondwana was the Araçuaí-West Congo orogen, which is a > 500 km wide (Alkmim et al., 2006) hot orogen (Vauchez et al., 2019).

The long-lived hot character of this orogen is well-registered in a widespread mid-to-lower anatectic crust and the source of high heat supply is often related to slab-breakoff (Bento dos Santos et al., 2015; Gradim et al., 2014). As it is shown in our models, during 300 Myr of tectonic quiescence in wide orogenic lithospheres, less than half of the period is dominated by conductive cooling (Fig. 4), which means that more than 200 Myr of advective heating during tectonic quiescence could explain the hot orogenic character, not excluding slab breakoff or other sources of heat, but adding even more heat to the base of the orogenic lithosphere. The Araçuaí-West Congo orogen can be an example showing that not only structural inheritance (i.e. crustal and lithospheric-scale faults) but also rheological inheritance due to adjacent cratonic and orogenic domains is an important factor controlling post-quiescence reactivation of ancient orogens during supercontinent rifting.

As it was pointed out in subsection 5.2, highly viscous continental lithosphere tends to increase the $\Delta\rho$ threshold between inward and outward flow. The higher this limit, the higher the tendency of outward flow, which results in sharp lithospheric thickness variations after periods of tectonic quiescence. This sharp variation in lithospheric thickness is observed by seismic tomography in different cratonic margins, such as the Colorado Plateau, Western Canada and Sorgenfrei-Tornquist zone in northern Europe (Currie and van Wijk, 2016). We conclude that the preservation of these sharp transitions can be obtained not only by a compositional increase of the viscosity of the lithospheric mantle, but also by the decrease in $\Delta\rho$.

6. Conclusions

The lateral flow of adjacent cratonic and orogenic lithosphere was here simulated in terms of density contrasts and adjacent thin lithosphere width during a long-lived period of tectonic quiescence. Our conclusions are the following:

- $\Delta\rho$ variations between lithospheric and sublithospheric mantle largely control the shape of the marginal cratonic lithosphere in respect to the adjacent thinner lithosphere, either by inward flow (e.g. underplating of cratonic lithosphere beneath an orogenic domain) or by outward flow (e.g. erosional edge-driven convection).
- The viscosity of the lithospheric mantle controls the threshold between underplating and erosional edge-driven convection in wide mobile belts. Highly viscous cratonic margins tend to preserve the

sharp thickness variations between cratons and mobile belts after tectonic quiescence.

- The width of the mobile belt (thinner lithosphere) has major effects on its rheology during its evolution under tectonic quiescence. For widths < 300 km, the inward flow causes it to strengthen, whereas outward flow allows otherwise. For wide mobile belts (> 300 km), most of the thinner lithosphere is highly influenced by lengthy advective heating, which favors lithospheric softening.
- Strengthening or softening of the mobile belt lithosphere adjacent to cratonic lithosphere can be envisaged as a type of rheological inheritance that can influence the response of large continental lithospheric blocks (e.g. supercontinents) to tectonic processes such as rifting or orogenesis.
- Since $\Delta\rho$ variations have shown to largely affect juxtaposed cratonic and orogenic lithospheric flows, experimentally-derived density values should be favoured in numerical simulations due to their age dependence, which is important for the mantle-lithosphere dynamics during the geodynamic evolution of Earth.

Author statement

Salazar-Mora, C.A.: Conceptualization, Methodology, Validation, Formal analysis, Writing – Original Draft,

Sacek, V.: Conceptualization, Methodology, Software, Writing – Review & Editing, Funding Acquisition

Declaration of Competing Interest

The authors declare that they have no known competing financial interests or personal relationships that could have appeared to influence the work reported in this paper.

Acknowledgements

The authors would like to thank financial support from FAPESP (projects 2017/10467-4 and 2017/24870-5) and Petrobras (project 2017/00461-9). We would also like to thank two anonymous reviewers for their constructive comments that greatly improved our manuscript.

Appendix A. Supplementary data

Supplementary material related to this article can be found, in the online version, at doi:10.1016/j.jog.2021.101830.

References

- Alkmim, F.F., Marshak, S., Pedrosa-Soares, A.C., Peres, G.G., Cruz, S.C.P., Whittington, A., 2006. Kinematic evolution of the Araçuaí-West Congo orogen in Brazil and Africa: nutcracker tectonics during the Neoproterozoic assembly of Gondwana. *Precambrian Res.* 149, 43–64. <https://doi.org/10.1016/j.precamres.2006.06.007>.
- Artemieva, I.M., 2011. *The lithosphere: An Interdisciplinary Approach*. Cambridge University Press, Cambridge.
- Artemieva, I.M., Mooney, W.D., 2002. On the relations between cratonic lithosphere thickness, plate motions, and basal drag. *Tectonophysics* 358, 211–231. [https://doi.org/10.1016/S0040-1951\(02\)00425-0](https://doi.org/10.1016/S0040-1951(02)00425-0).
- Audet, P., Bürgmann, R., 2011. Dominant role of tectonic inheritance in supercontinent cycles. *Nat. Geosci.* 4, 184–187. <https://doi.org/10.1038/ngeo1080>.
- Balay, S., Abhyankar, S., Adams, M., Brown, J., Brune, P., Buschelman, K., Dalcin, L., Dener, A., Eijkhout, V., Gropp, W., Karpayev, D., Kaushik, D., Knepley, M., May, D., McInnes, L.C., Mills, R., Munson, T., Rupp, K., Sanan, P., Smith, B., Zampini, S., Zhang, H., Zhang, H., 2018. *PETSc Users Manual*. Revision 3.10. Argonne, IL (United States). <https://doi.org/10.2172/1483828>.
- Bento dos Santos, T.M., Tassinari, C.C.G., Fonseca, P.E., 2015. Diachronic collision, slab break-off and long-term high thermal flux in the Brasiliano–pan-African orogeny: implications for the geodynamic evolution of the Mantiqueira Province. *Precambrian Res.* 260, 1–22. <https://doi.org/10.1016/j.precamres.2014.12.018>.
- Burov, E.B., Diament, M., 1995. The effective elastic thickness (T_e) of continental lithosphere: what does it really mean? *J. Geophys. Res. Solid Earth* 100, 3905–3927. <https://doi.org/10.1029/94JB02770>.
- Cainelli, C., Mohriak, W.U., 1999. Some remarks on the evolution of sedimentary basins along the eastern Brazilian continental margin. *Episodes* 22, 206–216.
- Chen, Y., Gu, Y.J., Currie, C.A., Johnston, S.T., Hung, S.H., Schaeffer, A.J., Audet, P., 2019. Seismic evidence for a mantle suture and implications for the origin of the Canadian Cordillera. *Nat. Commun.* 10, 1–10. <https://doi.org/10.1038/s41467-019-09804-8>.
- Currie, C.A., van Wijk, J., 2016. How craton margins are preserved: insights from geodynamic models. *J. Geodyn.* 100, 144–158. <https://doi.org/10.1016/j.jog.2016.03.015>.
- Doin, M.-P., Fleitout, L., Christensen, U., 1997. Mantle convection and stability of depleted and undepleted continental lithosphere. *J. Geophys. Res. Solid Earth* 102, 2771–2787. <https://doi.org/10.1029/96JB03271>.
- Foley, S.F., 2008. Rejuvenation and erosion of the cratonic lithosphere. *Nat. Geosci.* 1, 503–510. <https://doi.org/10.1038/ngeo261>.
- Gradim, C., Roncato, J., Pedrosa-Soares, A.C., Cordani, U., Dussin, I., Alkmim, F.F., Queiroga, G., Jacobsohn, T., Silva, L.C.Da, Babinski, M., 2014. The hot back-arc zone of the Araçuaí orogen, Eastern Brazil: from sedimentation to granite generation. *Brazilian J. Geol.* 44, 155–180. <https://doi.org/10.5327/Z2317-4889201400010012>.
- Green, D.H., Falloon, T.J., 1998. Pyrolyte: a Ringwood concept and its current expression. In: Jackson, I. (Ed.), *The Earth's Mantle: Composition, Structure, and Evolution*. Cambridge University Press, pp. 311–378. <https://doi.org/10.1017/CBO9780511573101.010>.
- Griffin, W.L., O'Reilly, S.Y., Ryan, C.G., Gaul, O.F., Ionov, D.A., 1998. Secular variation in the composition of subcontinental lithospheric mantle. In: Braun, Jean, Dooley, Jim, Goleby, Bruce, Klootwijk, C.T., V.D.H.R. (Eds.), *Structure and Evolution of the Australian Continent*. Geodynamic Series, 26., pp. 1–26. <https://doi.org/10.1002/9781118670095.ch1>.
- Gueydan, F., Précigout, J., Montési, L.G.J., 2014. Strain weakening enables continental plate tectonics. *Tectonophysics* 631, 189–196. <https://doi.org/10.1016/j.tecto.2014.02.005>.
- Heron, P.J., 2018. Mantle Plumes and Mantle Dynamics in the Wilson Cycle. *Geol. Soc. London, Spec. Publ.* <https://doi.org/10.1144/SP470.18>. SP470.18.
- Hieronymus, C.F., Shomali, Z.H., Pedersen, L.B., 2007. A dynamical model for generating sharp seismic velocity contrasts underneath continents: application to the Sorgenfrei-Tornquist Zone. *Earth Planet. Sci. Lett.* 262, 77–91. <https://doi.org/10.1016/j.epsl.2007.07.043>.
- Jordan, T.H., 1978. Composition and development of the continental tectosphere. *Nature* 274, 544–548. <https://doi.org/10.1038/274544a0>.
- Jordan, T.H., 1979. Mineralogies, densities and seismic velocities of garnet lherzolites and their geophysical implications. *The Mantle Sample: Inclusion in Kimberlites and Other Volcanics*. American Geophysical Union, Washington, D. C., pp. 1–14. <https://doi.org/10.1029/SP016p0001>.
- King, S.D., 2005. Archean cratons and mantle dynamics. *Earth Planet. Sci. Lett.* 234, 1–14. <https://doi.org/10.1016/j.epsl.2005.03.007>.
- King, S.D., Anderson, D.L., 1998. Edge-driven convection. *Earth Planet. Sci. Lett.* 160, 289–296. [https://doi.org/10.1016/S0012-821X\(98\)00089-2](https://doi.org/10.1016/S0012-821X(98)00089-2).
- Lee, C.-T.A., Luffi, P., Chin, E.J., 2011. Building and destroying continental mantle. *Annu. Rev. Earth Planet. Sci.* 39, 59–90. <https://doi.org/10.1146/annurev-earth-040610-133505>.
- Pearson, D.G., Wittig, N., 2014. The formation and evolution of cratonic mantle lithosphere – evidence from mantle xenoliths. *Treatise on Geochemistry*. Elsevier, pp. 255–292. <https://doi.org/10.1016/B978-0-08-095975-7.00205-9>.
- Peslier, A.H., Luhr, J.F., 2006. Hydrogen loss from olivines in mantle xenoliths from Simcoe (USA) and Mexico: mafic alkalic magma ascent rates and water budget of the sub-continental lithosphere. *Earth Planet. Sci. Lett.* 242, 302–319. <https://doi.org/10.1016/j.epsl.2005.12.019>.
- Peslier, A.H., Woodland, A.B., Bell, D.R., Lazarov, M., 2010. Olivine water contents in the continental lithosphere and the longevity of cratons. *Nature* 467, 78–81.
- Pollack, H.N., 1986. Cratonization and thermal evolution of the mantle. *Earth Planet. Sci. Lett.* 80, 175–182. [https://doi.org/10.1016/0012-821X\(86\)90031-2](https://doi.org/10.1016/0012-821X(86)90031-2).
- Poudjom Djomani, Y.H., O'Reilly, S.Y., Griffin, W.L., Morgan, P., 2001. The density structure of subcontinental lithosphere through time. *Earth Planet. Sci. Lett.* 184, 605–621. [https://doi.org/10.1016/S0012-821X\(00\)00362-9](https://doi.org/10.1016/S0012-821X(00)00362-9).
- Priestley, K., McKenzie, D., Ho, T., 2018. A lithosphere-asthenosphere boundary-a global model derived from multimode surface-wave tomography and petrology. *Lithospheric Discontinuities*, pp. 111–123. <https://doi.org/10.1002/978119249740.ch6>.
- Ringwood, A.E., 1975. *Composition and Petrology of the Earth's Mantle*, International Series in the Earth and Planetary Sciences. McGraw-Hill.
- Sacek, V., 2017. Post-rift influence of small-scale convection on the landscape evolution at divergent continental margins. *Earth Planet. Sci. Lett.* 459, 48–57. <https://doi.org/10.1016/j.epsl.2016.11.026>.
- Salazar-Mora, C.A., Huisman, R.S., Fossen, H., Egydio-Silva, M., 2018. The Wilson cycle and effects of tectonic structural inheritance on rifted passive margin formation. *Tectonics* 37, 3085–3101. <https://doi.org/10.1029/2018TC004962>.
- Schmitt, R., da, S., Fragoso, R., de, A., Collins, A.S., 2018. Suturing gondwana in the Cambrian: the orogenic events of the final amalgamation. In: Siegesmund, S., Basei, M.A.S., Oyhantcabal, P., Oriolo, S. (Eds.), *Geology of Southwest Gondwana*. Regional Geology Reviews. Springer International Publishing, Cham, pp. 411–432. <https://doi.org/10.1007/978-3-319-68920-3.15>.
- Şengör, A.M.C., Lom, N., Sağdıç, N.G., 2018. Tectonic Inheritance, Structure Reactivation and Lithospheric Strength: the Relevance of Geological History, 470. *Geol. Soc. London, Spec. Publ.* <https://doi.org/10.1144/SP470.8>. SP470.8.
- Solomatov, V.S., Moresi, L.-N., 2000. Scaling of time-dependent stagnant lid convection: application to small-scale convection on Earth and other terrestrial planets. *J. Geophys. Res. Solid Earth* 105, 21795–21817. <https://doi.org/10.1029/2000JB900197>.

van Keken, P.E., King, S.D., Schmeling, H., Christensen, U.R., Neumeister, D., Doin, M.-P., 1997. A comparison of methods for the modeling of thermochemical convection. *J. Geophys. Res. Solid Earth* 102, 22477–22495. <https://doi.org/10.1029/97JB01353>.

Vaucher, A., Hollanda, M.H.B.M., Monié, P., Mondou, M., Egydio-Silva, M., 2019. Slow cooling and crystallization of the roots of the Neoproterozoic Araçuaí hot orogen (SE

Brazil): implications for rheology, strain distribution, and deformation analysis. *Tectonophysics* 766, 500–518. <https://doi.org/10.1016/j.tecto.2019.05.013>.

Zhong, S.J., Yuen, D.A., Moresi, L.N., 2007. Numerical methods for mantle convection. In: Schubert, G. (Ed.), *Treatise on Geophysics*, Vol. 7. Elsevier, Amsterdam, pp. 227–252. <https://doi.org/10.1016/B978-044452748-6.00118-8>.